Proc. Natl. Acad. Sci. USA
Vol. 79, pp. 106–107, January 1982
Biophysics

Energy-filtered transmission electron microscopy of ferritin

(energy-loss spectroscopy/analytical chemistry)

HENRY SHUMAN AND ANDREW P. SOMLYO

Pennsylvania Muscle Institute, Departments of Physiology and Pathology, University of Pennsylvania School of Medicine, Philadelphia, Pennsylvania 19104

Communicated by Robert E. Forster, September 10, 1981

ABSTRACT **The focusing properties of a magnetic-sector spectrometer are shown to be suitable for forming high-spatial-resolution, energy-filtered transmission electron microscope images. Filtered images of ferritin molecules by using electrons scattered from the characteristic iron $M_{2,3}$ and carbon K absorption edges clearly distinguish the 75-Å iron core and 120-Å protein shell. The minimum detectable mass is estimated to be 0.84×10^{-20} g for Fe for an electron dose of 18 C/cm^2 and 99% confidence.**

The visualization of the elemental composition of materials at ultrastructural resolution is a major aim of modern, analytical electron microscopy. Relatively high (10–20 nm) resolution images showing the distribution of some constituent elements have been obtained by imaging with characteristic x-rays produced by a scanning electron beam generated with a high-brightness field emission source (1–3). However, x-ray mapping is ultimately limited by the low-fluorescence yield of x-ray production and low-collection efficiency of x-ray detectors. Compositional imaging at higher resolution and with greater sensitivity should be attainable by imaging with electrons that have experienced characteristic energy losses within the specimen (4–8). Furthermore, such energy-loss images contain molecular, in addition to atomic, information (9).

To form energy-filtered images in otherwise conventional transmission electron microscopes, achromatic energy filters, such as the Castaing–Henry (10, 11) and Omega filters (12), have been used. These filters are complicated and require extensive modification of the microscope column that is not easily realizable on available high-vacuum microscopes. The simpler magnetic-sector spectrometer is not generally achromatic, and imaging with this type of spectrometer normally has been performed in a scanning transmission electron microscope (5, 7–9, 13). We shall demonstrate, however, that although the chromatic aberration of a single-sector spectrometer is large, high-resolution transmission electron microscopic images can be produced with it and that this method is also readily adaptable to high-vacuum transmission electron microscopes.

INSTRUMENTATION

The sector used for filtered imaging is double focusing and was corrected for second-order aberrations at the energy-dispersion plane (14). Its use as a spectrometer and spectrograph has been described (14, 15). A schematic diagram of the median-plane focal properties are shown in Fig. 1. The energy-dispersing object plane, designated OP_1, of the spectrometer coincides with the back focal plane of the microscope (Philips EM400) imaging lens. This plane is focused by the magnetic sector to the dispersive image plane, designated IP_1. An energy-selecting slit placed at IP_1 allows an energy-loss spectrum of a selected area of the specimen to be generated by changing the magnetic field in the sector. Other planes between OP_1 and the magnetic sector entrance are focused to first order by the spectrometer. In particular, the object plane OP_2, corresponding to the microscope viewing screen, is focused at the image plane IP_2. For the sector described (14), IP_2 is 23 cm behind the energy-selecting slits, and there a real energy-filtered image is formed. By placing a transmission phosphor at this plane, the filtered images can be observed with the silicon intensified target (SIT) vidicon as described (15). The high sensitivity of the SIT tube allows real-time observation of the energy-filtered images. The vidicon's associated electronics (PAR OMA-2) digitizes and accumulates multiple television frames for subsequent numerical processing.

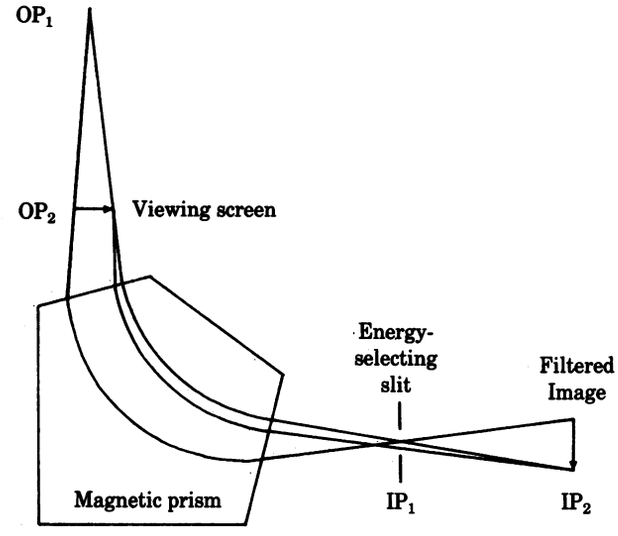

FIG. 1. Schematic diagram of ray paths of electrons in a magnetic-sector spectrometer.

ABERRATIONS

The simple sector spectrometer obviously does not meet the requirements of a low-aberration projector lens and is far from perfect. However, because the overall spatial resolution of the scintillator, light optics, and the SIT tube at IP_2 is only 50 μm, most of the aberrations are not observed. The spatial resolution-limiting aberrations are astigmatism and transverse chromatic aberration. The sector astigmatism can be corrected with the microscope objective lens stigmators. The transverse chromatic aberration is not correctable and is a consequence of the finite energy dispersion of the sector. Measured at IP_2, the chromatic effect is 6 μm/eV. For an energy-selecting width of 5 eV, a point image at OP_2 will be blurred in the dispersion direction

The publication costs of this article were defrayed in part by page charge payment. This article must therefore be hereby marked "*advertisement*" in accordance with 18 U. S. C. §1734 solely to indicate this fact.

Abbreviation: SIT, silicon intensified target.

to 30 μm at IP_2. The magnification of the sector is $\times 0.75$ in the dispersion direction and $\times 1.1$ in the perpendicular direction. Therefore, the spatial resolution at the specimen for this energy width is limited by the television-system resolution and microscope magnification.

RESULTS

The ferritin molecule has been used to test the sensitivity of x-ray (16) and energy-loss (5, 13, 17) microanalysis. The molecule has a 12-nm-diameter outer protein shell and an inner iron oxide hydrate core that is 7.5 nm in diameter (18). The core contains up to $\approx$5000 iron atoms composing 25% of the total mass of the molecule. Energy-filtered transmission electron microscopic images of ferritin are shown in Fig. 2 for three energy losses. The electron-microscope magnification for Fig. 2 was $\times$17,000, giving a resolution of 4 nm in the dispersion direction and 2.7 nm in the perpendicular direction. The iron $M_{2,3}$ absorption edge occurs at an energy loss of 54 eV. Fig. 2*A* was taken below this edge with electrons that had lost 45–50 eV of energy, Fig. 2*B*, with electrons that had lost 55–60 eV; and Fig. 2*D* at the carbon K edge, with electrons that had lost 290–295 eV. The contrast in Fig. 2*A* is primarily due to inelastic background scattering from carbon in the protein shell and oxygen in the core, whereas the contrast in Fig. 2*B* is due to carbon, oxygen, and iron. In Fig. 2*D*, the contrast is due to the distribution of carbon and partially to the loss of electrons by large-angle elastic scattering from the iron core. The 7.5-nm "vacancy" due to the iron core is clearly resolved. The images in Fig. 2 *A* and *B* have been scaled so that the carbon-support film appears with equal intensity. The two pictures can be subtracted to give an image only due to iron in the core as shown in Fig. 2*C*. The number of iron M-edge electrons detected over the ferritin core in Fig. 2*C* was $P = 1.7 \times 10^5$, whereas in the same region of Fig. 2*A* there were $B = 9.3 \times 10^5$ background electrons detected. If the accuracy of the image subtraction is determined by counting statistics, signal-to-noise ratio S/N for detecting iron in the core is

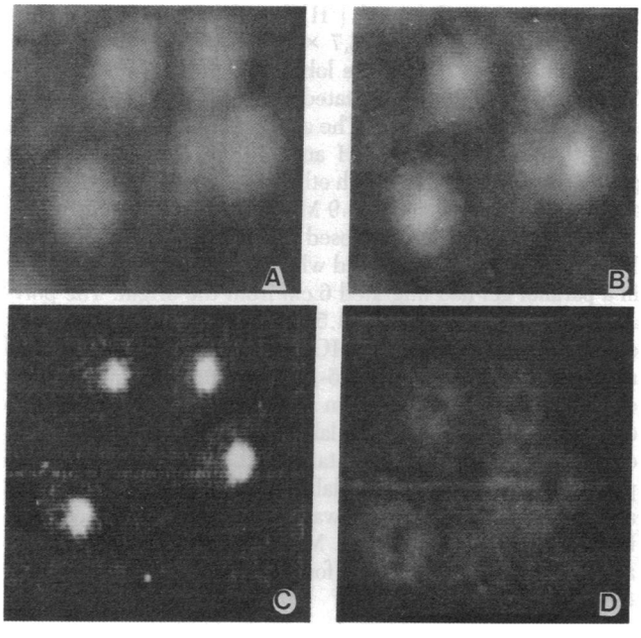

FIG. 2. Digitally recorded energy-filtered electron micrographs of ferritin molecules. Images A, B, and D were formed with electrons that had lost 45–50 eV, 55–60 eV, and 290–295 eV of energy, respectively. Image C is the difference between images A and B.

$$S/N = \frac{P}{(B+P)^{1/2}} = \frac{1.7 \times 10^5}{(1 \times 10^6)^{1/2}} = 170,$$

or the number of iron atoms in the core is

$$N \pm \sigma_n = 5000 \pm 30 \text{ atoms},$$

where σ_n is the predicted standard deviation and $3 \times \sigma_n$ is the minimal detectable mass. The current density at the specimen for the pair of 5-sec exposures was 1.8 a/cm^2 for a total dose of 18 C/cm^2. Single iron-atom detection at an equal mass fraction of iron to carbon would require 1.4×10^5 C/cm^2, for a 99% confidence limit.

CONCLUSION

A simple magnetic sector designed as an electron spectrograph can be used as an imaging filter. The large transverse chromatic aberration of the sector limits the image resolution to $\approx$40 μm, referred to the microscope viewing screen for an energy-filtered width of 5 eV. For low-lying, closely spaced absorption edges, this aberration is not a severe limitation, and the 7-nm Fe core and surrounding organic shell of the ferritin molecule are readily resolved. The digitally recorded image has the advantage that corrections for background effects can be obtained through subtraction of a pre-edge image from the image obtained with characteristic energy-loss electrons. We further suggest that the use of "complementary energy-loss images" in regions of elemental segregation (e.g., iron and carbon energy-loss images in ferritin) are useful in excluding features due to spurious contrast caused by variations in mass density. The minimum detectable mass, as has been demonstrated (5), is of the order of 100 atoms for high-density electron exposures.

This work was supported by National Institutes of Health Grant HL15835 to the Pennsylvania Muscle Institute.

1. Somlyo, A. P., Somlyo, A. V., Shuman, H. & Stewart, M. (1979) in *Scanning Electron Microscopy*, ed. O. Johari, pp. 711–722.
2. Stewart, M., Somlyo, A. P., Somlyo, A. V., Shuman, H., Lindsay, J. A. & Murrell, W. G. (1980) *J. Bacteriol.* **143**, 481–491.
3. Somlyo, A. V., Gonzalez-Serratos, H., Shuman, H., McClellan, G. & Somlyo, A. P. (1981) *J. Cell Biol.* **90**, 577–594.
4. Isaacson, M. S. & Crewe, A. V. (1975) *Annu. Rev. Biophys. Bioeng.* **4**, 165–184.
5. Isaacson, M. & Johnson, D. (1975) *Ultramicroscopy* **1**, 33–52.
6. Egerton, R. F. (1978) *Ultramicroscopy* **3**, 243–251.
7. Hren, J. J., Goldstein, J. I. & Joy, D. C. eds. (1979) *Introduction to Analytical Electron Microscopy* (Plenum, New York), pp. 223–242.
8. Shuman, H., Somlyo, A. V. & Somlyo, A. P. (1980) in *Microbeam Analysis*, ed. Wittry, D. B. (San Francisco Press, San Francisco), pp. 275–279.
9. Hainfeld, J. & Isaacson, M. (1978) *Ultramicroscopy* **3**, 87–95.
10. Castaing, R. & Henry, L. (1962) *C. R. Hebd. Acad. Seances Sci.* **255**, 76–78.
11. Ottensmeyer, F. P., Bazett-Jones, D. P. & Adamson-Sharpe, K. M. (1980) in *Microbeam Analysis*, ed. Wittry, D. B. (San Francisco Press, San Francisco), pp. 280–282.
12. Krahl, D. & Herrmann, K.-H. (1980) *Micron* **11**, 287–289.
13. Colliex, C. & Trebbia, P. (1979) in *Microbeam Analysis in Biology*, eds. Lechene, C. & Warner, R. (Academic, New York), pp. 65–86.
14. Shuman, H. (1980) *Ultramicroscopy* **5**, 45–53.
15. Shuman, H. (1981) *Ultramicroscopy* **6**, 163–168.
16. Shuman, H. & Somlyo, A. P. (1976) *Proc. Natl. Acad. Sci. USA* **73**, 1193–1195.
17. Nomura, S., Todokoro, H. & Komoda, T. (1977) *J. Electron Microsc.* **26**, 277–283.
18. Massover, W. H. (1978) *J. Mol. Biol.* **123**, 721–726.